Perspective

MRC

Received: 25 January 2016 Revised: 10 February 2016 Accepted: 17 February 2016 Published online in Wiley Online Library: 29 March 2016

(wileyonlinelibrary.com) DOI 10.1002/mrc.4428

Parallel NMR spectroscopy with simultaneous detection of ^{1}H and ^{19}F nuclei

Helena Kovacs[a] and Ēriks Kupče[b]*

Introduction

New experimental techniques that have become feasible with the arrival of NMR instruments equipped with multiple receivers[1–5] allow a significant increase in the productivity and throughput in NMR laboratories dealing with structure elucidation and routine analysis of both, biomolecular systems[6] as well as small molecules in either liquids[7] or solids.[8] Here we attempt to highlight the possibilities of using the multi-receive experiments to increase the efficiency in analysis of molecules containing more than one species of sensitive nuclei. We particularly focus on combining the basic ^{1}H detected experiments with ^{19}F detection not least because of the important role that ^{19}F NMR plays in the drug discovery methodology and in the pharmaceutical industry in general.[9–16] Furthermore, the combination of the two of the most sensitive and abundant NMR nuclei is ideal for exploring new avenues in multi-receive experiment design, testing new pulse sequences and following the coherence transfer pathways in complex spin networks that form the basis of modern multi-dimensional NMR experiments.

In the drug discovery research low molecular weight compounds in large numbers are screened to establish their potential to interact with a target protein.[9–12] The compound repositories used for target screening may contain up to 20% fluorinated substances and also numerous common drugs contain fluorine atoms.[13] The reason for the presence of fluorine in the compound libraries and pharmaceuticals is the favourable effect of fluorine substitution on the biological activity of small molecules, as it may render, for instance, higher metabolic stability, increased bioavailability through better membrane permeability or enhanced affinity for the target enzyme.[14,15] In addition, ^{19}F-detected NMR is gaining popularity as an analytical tool for the fragment-based drug design thanks to the high sensitivity of the fluorine atom to its local environment that manifests through changes both in ^{19}F chemical shift and the line width upon target binding.[16] Consequently, it becomes necessary to include fluorine atoms in the structural investigations of the compounds and the binding epitopes.

Fluorine is a very popular NMR nucleus not only because of its high natural abundance and NMR sensitivity that is inferior only to that of protons but also because of a large chemical shift range and excellent signal dispersion. With a minor adjustment of parameters to the slightly different values of scalar couplings and the ^{19}F gamma ratio most of the pulse sequences that are used for proton-detected experiments can be easily adapted for research involving direct ^{19}F observation.[17] The multi-receiver technology allows combining the best of both worlds making ^{1}H and ^{19}F detected NMR experiments even more efficient. Yet the multi-receive experiments that have been developed for spin systems involving two or more abundant high-sensitivity nuclei remain underutilized.[18–20] We show that in sampling limited situations the use of parallel acquisition can potentially increase throughput in NMR laboratories working with fluorine containing compounds by at least a factor of two. This comes close to having an extra spectrometer in an NMR laboratory for free. On the other hand, in sensitivity limited situations multi-receive experiments have a potential to increase the sensitivity of measurements because more signal is acquired per unit time. Furthermore, the polarization that is often discarded on systems equipped with a single receiver can be detected and utilized in experiments involving multiple receivers.

In this work we demonstrate and discuss a variety of experiments designed for NMR systems equipped with multiple receivers. We focus on three basic types of such experiments and the main principles of designing pulse sequences for multi-receiver systems. We briefly illustrate the compatibility of such experiments with other state-of-the-art techniques for speeding up NMR experiments, such as Hadamard encoding,[21] non-uniform sampling,[22] computer optimized folding,[23,24] relaxation optimized experiments[25] and spatial encoding techniques.[26,27] Undoubtedly, many of the experiments presented here can be further improved, developed and extended to more complex spin systems and to a larger number of simultaneous experiments and/or simultaneously detected nuclear species. This work aims at stimulating such developments.

Three types of experiments for two receivers

Based on their design features the experiments involving two receivers can be categorized into three main types: (i) interleaved experiments, (ii) parallel acquisition experiments, and (iii) sequential acquisition experiments. A simple illustrative example of each type of such experiments is shown in Fig. 1.

The three types of experiments have different limitations, design features and the achievable efficiency. For instance, in parallel acquisition experiments (Fig. 1b) mutual decoupling of *A* and *X* nuclei during direct observation is usually not feasible. On the other hand, in the interleaved (Fig. 1a) and sequential acquisition experiments (Fig. 1c) mutual decoupling of *A* and *X* nuclei is feasible, but may affect the efficiency of the experiments as discussed in detail in the succeeding texts. Note also that the PANSY (Parallel Acquisition NMR SpectroscopY) experiments[2] (Fig. 1b,c) often share an

* Correspondence to: Ēriks Kupče, Bruker UK Limited, Banner Lane, Coventry CV4 9GH, UK. E-mail: eriks.kupce@bruker.com

a Bruker BioSpin AG, Industriestrasse 26, CH-8117, Fällanden, Switzerland

b Bruker UK Limited, Banner Lane, Coventry CV4 9GH, UK

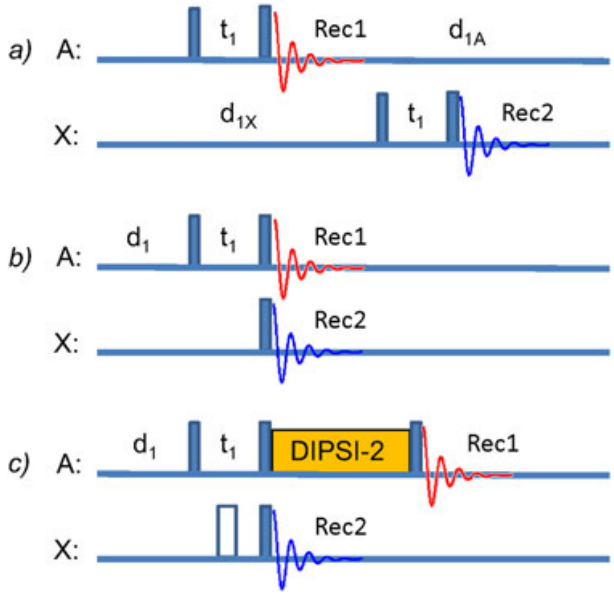

Figure 1. Examples of the three types of experiments involving two receivers: (a) interleaved experiments,[28] e.g. interleaved COSY (A-A COSY and X-X COSY); (b) parallel acquisition experiments,[2] e.g. PANSY-COSY (A-A COSY and A-X COSY); and (iii) sequential acquisition experiments,[2] e.g. PANSY-TOCSY (2D A-A TOCSY and 1D X NMR).

evolution period and therefore can have one or more *joint* frequency axis in the indirectly detected dimension(s). On the other hand, the interleaved experiments (Fig. 1a) can only have *separate* evolution periods that may or may not involve the same frequency domain.

The total duration of a typical NMR experiment, T_{tot}, is given by a sum of three main time periods – the pulse sequence (τ_{pp}), the acquisition period (τ_{aq}) and the recovery period (d_1), multiplied by the total number, n of directly acquired free induction decays (FID's)

$$T_{tot} = n\left(d_1 + \tau_{pp} + \tau_{aq}\right) \quad (1)$$

Therefore, the time saving, η, that is achieved in a multi-receive/multi-FID experiment of total duration, $T_{tot}(MF)$, is generally given by

$$\eta = \frac{\sum_{i=1}^{N} T_{tot}(i)}{T_{tot}(MF)} \quad (2)$$

where N is the number spectra recorded by the conventional method and $T_{tot}(i)$ is the total experiment time of the conventional experiments recorded sequentially with $i = 1,2,\ldots,N$ (refer to Fig. 2a for $N = 2$). It is common to ignore the sensitivity issues in fast techniques if the experiment time is said to be sampling limited rather than sensitivity limited. Stated otherwise, the duration of a two-dimensional (2D) experiment is determined by the number of t_1-increments needed to obtain the required resolution and not by the number of scans that is needed to achieve sufficient signal-to-noise ratio. In many applications the multi-receive experiments involving direct observation of abundant high-gamma nuclei, such as ^{1}H, ^{19}F and ^{31}P, are indeed sampling limited rather than sensitivity limited. Generally, the multi-FID experiments can involve direct observation of one or more NMR nuclei. Multi-receive experiments with up to five simultaneously detected nuclei (including deuterium) have been previously reported.[4,5] In this manuscript we focus on experiments involving simultaneous detection of two abundant and highly sensitive nuclei, ^{1}H and ^{19}F. Many of the experiments discussed in the succeeding texts can be (and in many

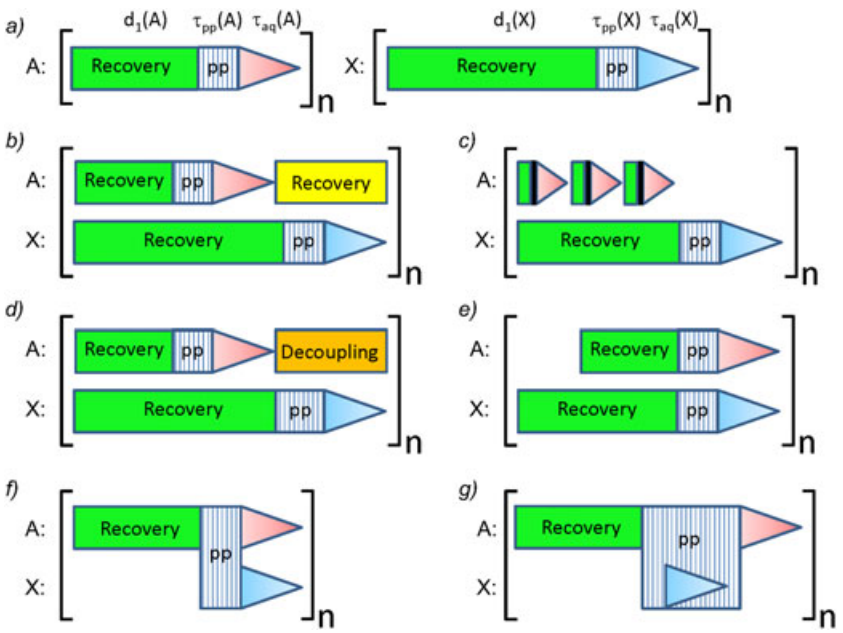

Figure 2. Various types of experiments involving two receivers: (a) the conventional way of acquiring A- and X-detected NMR spectra sequentially; (b) interleaved acquisition of two experiments with comparable recovery delays, d_1 for A and X nuclei, $d_{1A} \leq d_{1X}$; (c) interleaved acquisition experiments with very different A and X recovery delays, $d_{1A} \ll d_{1X}$; (d) interleaved acquisition experiments with decoupling of A nuclei, $d_{1A} \leq d_{1X}$; (e) parallel acquisition experiments with no polarization transfer between A and X; (f) parallel acquisition experiments with polarization transfer from A to X; (g) sequential acquisition experiments with polarization transfer from A to X and direct observation of the FID of X nuclei during the pulse sequence. All pulse sequences are repeated n times in the course of each individual experiment.

cases have been) implemented with direct observation of $^{1}H/^{31}P$ or (less common) $^{19}F/^{31}P$ pair of nuclei.

With this in mind we shall discuss the multi-FID/multi-receive experiments according to the three main types mentioned in the preceding texts, i.e. interleaved experiments, parallel acquisition experiments and sequential acquisition experiments. Within each type the multi-receive experiments can have various specific design features as shown, for instance in Fig. 2b–g.

The interleaved experiments (Fig. 2b–d) also known as Unified Time-Optimized Interleaved Acquisition (UTOPIA)[28] typically involve two or more 'independent' spin systems where the individual experiments are designed in such a way as to avoid mutual interferences. In a typical interleaved experiment magnetization of the passive nuclei is essentially undisturbed during the experiment involving the active nuclei and the time saving is achieved by allowing passive nuclear species *A* to recover while the experiment involving active nuclei *X* is carried out and vice versa (Fig. 2b). Any coherence exchange between the two directly observed nuclear species is usually avoided. In practice, the involved spin systems are often not completely isolated. Scalar couplings, dipolar couplings or cross relaxation may be present and have to be considered in order to maximize the performance of the interleaved experiments. For instance, the H-H COSY and F-F COSY experiments (Fig. 1a) can be recorded in an interleaved fashion with essentially no compromise in the performance. Assuming that in such experiments the recovery delay, d_1, is the longest time period and the recovery delays, $d_1(A)$ and $d_1(X)$, are comparable, the maximum time saving by a factor of 2 can be achieved. However, if the relaxation properties of the two nuclear species are substantially different, as, for instance, is often the case with ^{1}H and ^{13}C detected experiments (Fig. 2b), the time saving factor η is determined by the slowest of the two experiments:

$$\eta = \frac{T_{tot}(H) + T_{tot}(C)}{T_{tot}(C)} \quad (3)$$

For instance, assuming that the relaxation time $T_1(A) < T_1(X)$, the additional recovery period (shown in yellow in the electronic version of the manuscript) following the acquisition of the FID(A) are not necessary in the conventional experiment (Fig. 2a), but cannot be excluded in the interleaved experiment (Fig. 2b). On the other hand, if the two nuclei have very different relaxation properties and one of the experiments is considerably shorter, e.g. $T_{tot}(A) \ll T_{tot}(B)$ several FIDs of nuclei *A* can be accommodated inside the relaxation period of nuclei *X* (Fig. 2c). For example, this situation may be encountered if one nuclear species of a multi-receiver experiment are fast relaxing quadrupolar nuclei, such as ^{14}N or ^{17}O.

Note that no mutual decoupling of the two nuclear species was considered so far. While decoupling can easily be implemented (Fig. 2d) it clearly disturbs the passive spin system(s) as far as the interleaved multi-receive experiments are concerned. Assuming that the two nuclear species have a comparable relaxation properties, $T_1(A) \approx T_1(X)$, and the decoupling is applied only in one of the two experiments, e.g. to decouple spins *A* during the detection of spins *X*, the efficiency of the interleaved experiments is reduced because decoupling saturates the passive spins, *A*, and therefore a longer recovery delay $d_1(A)$ is now required. Furthermore, if decoupling is applied in both interleaved experiments the speed advantage is completely lost.

On the other hand, if the relaxation properties of the two nuclear species are significantly different, e.g. $T_1(A) < T_1(X)$ one can take advantage of the situation and decouple the fast relaxing nuclei, *A*, in both the direct and the indirect dimensions with no penalties with respect to the experiment duration, as shown in Fig. 2d. Both situations are encountered in the experiments described in the succeeding texts.

So far, we have ignored any interference effects between the two spin systems. However, such interference effects can be significant and must be considered. For instance, the two 'independent' spin systems may be affected by mutual scalar or dipolar couplings, cross-relaxation effects, pulse imperfections if, for instance, decoupling during the t_1 evolution is used, and similar. In fact, it has been shown that the cross-relaxation effects can be exploited to speed up acquisition.[25] Clearly, this opens opportunities for further research in the area of multi-receiver experiments..

While the interleaved experiments discussed in the preceding texts in principle can be implemented on single receiver systems by jumping the carrier frequency the advent of the multi-receiver technology enables a new type of pulse sequences that involve simultaneous (parallel) acquisition of several FIDs from two or more nuclear species (Fig. 1b).[2–5] The (PANSY) experiments may or may not involve coherence transfer between the directly detected nuclei (Fig. 2e,f). Just like in the interleaved experiments discussed in the preceding texts, in parallel acquisition experiments involving independent spin systems (Fig. 2f; no coherence transfer) the total experiment duration is determined by the longest of the two experiments. However, the parallel experiments typically are designed to take advantage of joint coherence transfer pathways and joint evolution periods, particularly in multi-dimensional and multi-nuclear pulse sequences. When coherence transfer from sensitive and relatively fast relaxing nuclei (e.g. ^{1}H) to insensitive, low-gamma nuclei (e.g. ^{13}C) can be utilized a significant increase in time saving is achieved (Fig. 2e):

$$\eta = \frac{\tau_{tot}(H) + \tau_{tot}(C)}{\tau_{tot}(H)} \quad (4)$$

where $\eta > 2$. One such example is the H,C′-N PANSY HSQC experiment that records H-N and C′-N 2D correlation experiments in parallel.[29] Assuming that $^{1}H_N$ nuclei relax twice as fast as the ^{13}C=O nuclei and the experiment times are dominated by the recovery delays $d_1(H)$ and $d_1(C')$ the two 2D spectra are recorded three times faster as compared with the two conventional H-N and C′-N correlation experiments whereas the interleaved experiments can be recorded only 1.5 times faster in this particular case. One drawback of the parallel acquisition experiments is that mutual decoupling of the A and X spins is usually not feasible.

Finally, in the sequential acquisition experiments (Fig. 1c) one or more FIDs are recorded within the pulse sequence by taking advantage of long J-evolution delays[30] or other coherence transfer periods such as TOCSY or NOESY mixing times.[2,31] This usually implies making use of joint coherence transfer pathways and involves one or more joint evolution periods. Incorporating direct observation periods into such experiments usually has little effect on the total duration of the pulse sequence and a time saving factor close to *N* can be achieved, where *N* is the number of acquired experiments. One such example is the PANACEA experiment that records several H-C and H-N HSQC and HMBC experiments simultaneously with the 2D C-C INADEQUATE spectra.[32,33]

In sequential acquisition experiments decoupling is feasible either by using the In-Phase Anti-Phase (IPAP) technique[30] or by taking advantage of the spin-lock (TOCSY or CPMG) periods.[2] One of the drawbacks of the sequential acquisition experiments is

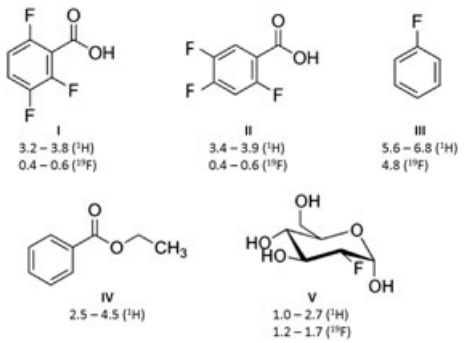

Scheme 1. Test molecules used in this work for multi-receive ^{1}H- and ^{19}F-detected experiments – 2,3,6-trifluoro-benzoic acid (**I**), 2,4,5-trifluoro-benzoic acid (**II**), fluoro-benzene (**III**), ethyl benzoate (**IV**), 2-fluoro-2-deoxy-glucose (**V**). The ^{1}H and ^{19}F T_1 relaxation time ranges (in seconds) were determined from parallel inversion-recovery experiments as described in the main text.

that the coherence transfer delays that are used for data acquisition may limit the available spectral resolution.

One of the significant advantages of the multi-receiver (PANSY) technique is that it allows observing magnetization from alternative coherence pathways that is often discarded or is unavailable for observation on the single receiver systems. In the case of experiments involving two sensitive nuclei such as ^{1}H and ^{19}F, magnetization from both nuclei can be observed simultaneously. Furthermore, in the conventional 2D experiments usually only one component of the magnetization following the t_1 evolution period is observed in each increment leading to a *sqrt*(2) loss in sensitivity. This sensitivity loss can be partially recovered in the so called sensitivity-enhanced experiments [34], but only if the following coherence transfer delay is sufficiently short (spin systems involving large one-bond scalar couplings). Multiple receivers allow utilizing of both components thus improving the efficiency of many conventional experiments, as we demonstrate in the succeeding texts.

In the succeeding texts we provide practical examples of various configurations of the three main types of multi-receive experiments. The test molecules used in this work are shown in Scheme 1.

Interleaved 2D experiments

In terms of the experiment design the interleaved ^{1}H and ^{19}F detected experiments are arguably the simplest type of multi-receiver experiments discussed in the preceding texts. The main design principle here is to avoid disturbing nuclei *A* while the experiment with direct detection of nuclei *X* is conducted and vice versa. This is relatively easily achieved in isolated spin systems with negligible *J* couplings between *A* and *X* nuclei. It should be pointed out that here we avoid discussing the effects of cross-relaxation because of lack of systematic studies about such effects in multi-receive experiments. Below we present three examples of interleaved experiments.

Interleaved H-H COSY and F-F COSY

One of the simplest and at the same time also the most useful experiments that can easily be adopted for interleaved acquisition is the 2D double-COSY experiment shown in Fig. 3a. In practice, we use two standard COSY pulse sequences with gradient coherence selection[34] (Fig. 3). The two pairs of matching gradients ($2\times$g1 and $2\times$g2) have different amplitudes to avoid any accidental refocussing of unwanted magnetization. The total repetition time for both COSY sequences is determined by the longest T_1 relaxation time of the two nuclear species, which in the test sample used here (mixture of compounds I–IV; Scheme 1) is protons. Therefore, the d_1 delay is set to half the usual proton recovery delay, i.e. 1 s. Because of the considerably shorter ^{19}F T_1 relaxation times in the chosen test sample the ^{19}F decoupling can be used to improve the resolution and sensitivity of the H-H COSY spectra with essentially no time penalty, as shown in Fig. 3b. Note that in the latter case the ^{19}F recovery delay is only as long as $d_1(F)$ delay. Because of the relatively fast ^{19}F T_1 relaxation the chosen $d_1(F) = 1$ s in this experiment is still sufficiently long for efficient ^{19}F recovery. On the other hand, the proton recovery is unperturbed throughout the F-F COSY experiment and the total recovery time for protons, $\tau_{rec}(H)$, is the same as in the experiment without ^{19}F decoupling:

$$\tau_{rec}(H) = \tau_{aq}(H) + T_{tot}(F) + d_1(H) \qquad (5)$$

i.e. ~2.5 *s*. There is more flexibility available for optimizing this experiment to fit the relaxation properties of the two nuclear species. For samples with somewhat longer ^{19}F T_1 relaxation the $d_1(F)$ delay can be increased at the expense of shortening the $d_1(H)$ delay while keeping the overall duration of the experiment constant.

The H-H COSY and F-F COSY spectra of a mixture containing compounds I–IV (Scheme1) recorded in 25 min using the pulse sequence of Fig. 3b are shown in Fig. 4. The longer relaxation time of fluoro-benzene was disregarded in this experiment because no F-F cross-peaks are expected for this molecule. As can be seen in Fig. 4b the dispersion of the ^{19}F signals is high and the fine structure of the individual ^{19}F signals is unresolved. Therefore, the ^{1}H decoupling in this experiment is not really necessary for the chosen test sample. In samples where ^{1}H decoupling is crucial for improving resolution and sensitivity of the F-F COSY spectra this particular experiment may not provide any significant advantages over recording the two COSY spectra sequentially in the conventional fashion.

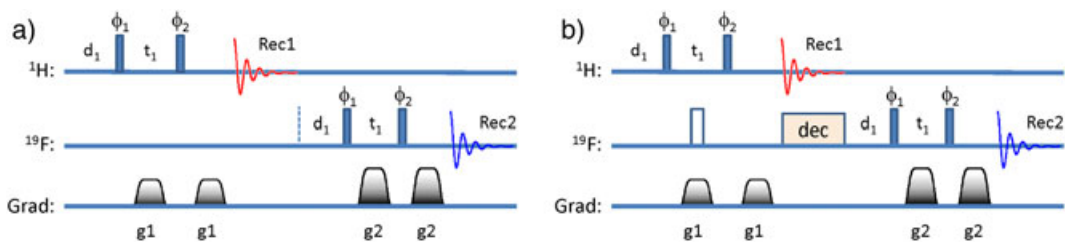

Figure 3. The pulse sequences for recording interleaved 2D H-H and F-F COSY spectra, (a) without decoupling and (b) with ^{19}F decoupling; phase cycling: $\varphi_1 = x, -x$; $\varphi_2 = x, x, -x, -x$, *Rec1* = *Rec2* = $x, -x$; gradients (ms, G/cm) g1 = (1.0, 21), g2 = (1.0, 27); the hollow rectangle is a 180° pulse with phase *x*. Adiabatic CA WURST-20 decoupling with 8 ms inversion pulse duration and 80 ppm bandwidth was used in the sequence (b).

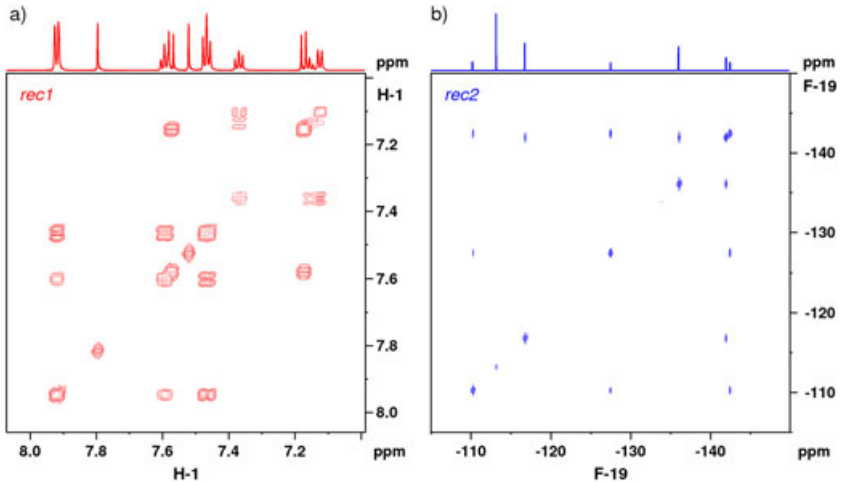

Figure 4. (a) H-H COSY and (b) F-F COSY spectra of a mixture of compounds I, II, III and IV in DMSO-d_6 recorded simultaneously on a 700 MHz Avance III HD spectrometer equipped with two receivers using the pulse sequence shown in Figure 3b. The raw data matrix size was 1024 (complex) × 512 × 512 data points, one scan per increment, experiment time was 25 min.

H/F DOSY

The DOSY experiment[35] enables NMR analysis of mixtures based on the size and molecular weight of molecules. Because of high sensitivity of proton NMR such measurements are typically carried out with ^{1}H detection. Unfortunately, the resolving power and accuracy of the DOSY measurements are severely hampered by signal overlap.[36] This is often the case in ^{1}H NMR spectra. Therefore, the ^{19}F NMR is particularly attractive choice for such measurements where applicable. On the other hand, in practice, the mixtures that are investigated may also contain molecules with no fluorine atoms and both ^{1}H and ^{19}F DOSY experiments can provide important complementary information in such cases. Therefore, simultaneous recording of ^{1}H and ^{19}F DOSY spectra would seem to be an excellent undertaking, not least because both experiments are acquired at exactly the same experimental and environmental conditions. The interleaved H/F DOSY pulse sequences are shown in Fig. 5. Two pairs of adiabatic ^{19}F pulses, a1 and a2, have opposite sweep direction and replace the conventional square refocussing pulses in the ^{19}F pulse sequence to avoid strong and cumulative off-resonance effects.[37]

The spectra of the mixture of compounds I–IV (Scheme 1) recorded using the interleaved DOSY pulse sequence of Fig. 5 are shown in Fig. 6. The repetition rate of this experiment is determined by the slowest relaxation rate, i.e. proton T_1 in this sample. Therefore, the recycling delay, d_1, was set to 3 s to ensure good quality spectra. In the ^{19}F DOSY spectra (Fig. 6b) the signals from tri-fluoro-benzoic acids I and II that have the same molecular weight line up perfectly and are easily distinguished from fluoro-benzene (III) that has much higher mobility. Overall, the signals are also well separated in the ^{1}H DOSY spectra (Fig. 6a), except for the proton in the para-position in fluoro-benzene (III), which overlaps with one of the signals from compound I (Scheme 1). More importantly, the ^{1}H and ^{19}F signals from this spectrum can be correlated and assigned because both spectra have a common F1 (diffusion) axis. Therefore, the combination of the two DOSY spectra recorded in a single (interleaved) experiment gives a deeper and more complete insight into the composition of this mixture as compared to the individual DOSY spectra.

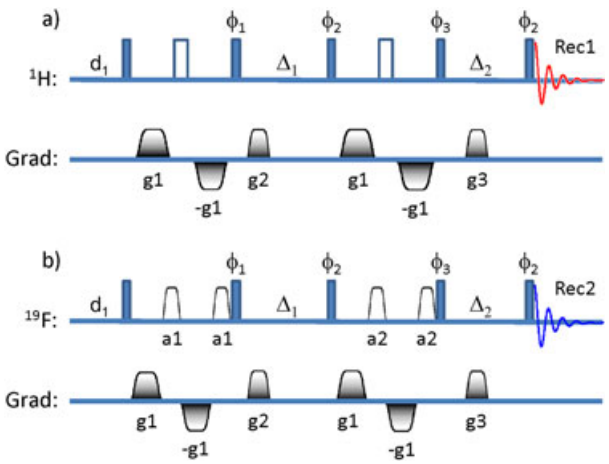

Figure 5. The interleaved DOSY experiment for simultaneous recording of the ^{1}H (a) and ^{19}F (b) DOSY spectra. Both sequences are applied in an interleaved mode as outlined in Figure 2b; delays: $d_1 = 3$ s, $\Delta_1 = 160$ ms, $\Delta_2 = 5$ ms; phase cycling: $\varphi_1 = x, x, -x, -x$, $\varphi_2 = 4(x), 4(-x)$, $\varphi_3 = 2(x, -x), 2(-x, x)$, *Rec1* = *Rec2* = $x, -x, -x, x, -x, x, x, -x$; gradients (ms, G/cm): *g1* = (2, 53.5), *g2* = (0.345, 9.16), *g3* = (0.345, 7.05). In (b) adiabatic CA-WURST pulses (1 ms, 140 ppm), a1 and a2 with opposite sweep direction replace the conventional rectangular refocussing pulses.

H-C and F-C HMQC

The H-C and F-C correlated experiments with multi-receiver detection can be recorded both in interleaved or in parallel acquisition arrangements. The interleaved version of the simultaneous ^{1}H- and ^{19}F-detected ^{13}C HMQC pulse sequence is shown in Fig. 7. A pair of adiabatic ^{13}C inversion pulses replaces the conventional refocusing pulses as shown in Fig. 7b to avoid strong artefacts caused by rectangular 180° pulses because of miscalibration and the off-resonance effects. Since in the test compounds I–IV studied here the T_1 relaxation of the ^{19}F nuclei on average is significantly faster than that of protons the ^{19}F decoupling can be used in the H-C HMQC part of the experiment with no penalties regarding the duration of the experiment, as discussed in the preceding texts for the COSY experiment. Once again, the proton recovery is undisturbed essentially for the duration of the whole experiment minus

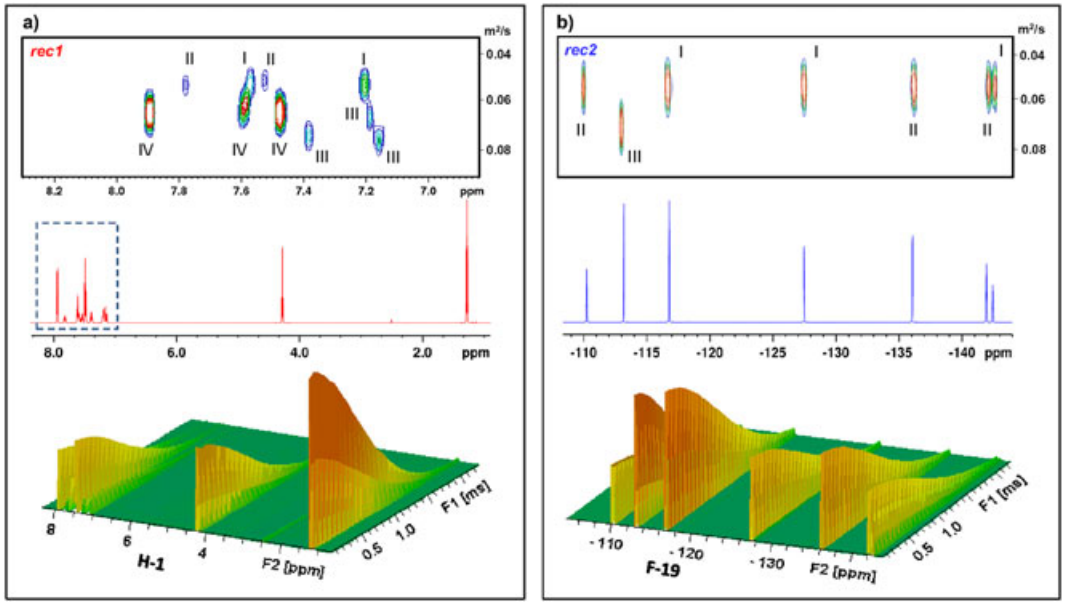

Figure 6. ^{1}H (a) and ^{19}F (b) DOSY spectra of a mixture containing compounds I–IV in DMSO-d_6, both recorded in an interleaved experiment using the pulse sequence shown in Fig. 5; 32 increments, 8 scans per increment.

the duration of the H-C HMQC pulse sequence (Eqn (5)). Note that although the ^{1}H-detected part of the experiment in the pulse sequence of Fig. 7 is shown first, in practice, it does not matter in which order the pulse programme is coded because the experiment is *cyclic*.

Depending on the relaxation properties of the two nuclear species in a particular sample of interest the duration of the $d_1(F)$ can be increased at the expense of reducing the $d_1(H)$ delay while the total duration of the experiment is unchanged (refer also to Fig. 1d). In the limit where the T_1 relaxation times of ^{1}H and ^{19}F nuclei become comparable, for instance in the compound V (Scheme 1), it is no more possible to accommodate ^{19}F decoupling without significantly increasing the duration of the experiment and ultimately losing any benefits from interleaved acquisition. The same penalties apply to decoupling of nuclei with the longest T_1 relaxation times, in this case protons. In this particular sample the ^{1}H decoupling was deemed unnecessary because of the high dispersion of the ^{19}F signals, relatively short ^{1}H acquisition times and the line broadening introduced by the applied window functions, rendering the H-F couplings unresolved in the F-C HMQC spectra.

Finally, it is worth mentioning that the power level of the ^{19}F decoupling can be significantly reduced by use of adiabatic decoupling sequences.[38] This is important because simultaneous ^{19}F and ^{13}C decoupling in fluorinated compounds may be problematic due to the very wide spectral ranges of both nuclei. The adiabatic decoupling can easily be adapted to the magnitude of the ^{1}H-^{19}F couplings that in the test molecules I–III do not exceed 25 Hz. Consequently, a 65.8 kHz (100 ppm) wide ^{19}F decoupling bandwidth was achieved using only 1.4 kHz (RMS) RF field strength.

The spectra recorded using the interleaved H/F-C HMQC pulse sequence of Fig. 7 are shown in Fig. 8. Note that each of the two experiments includes their own ^{13}C t_1 evolution period. In other words, the F1 frequency axis is not *shared* in the two spectra. It can be the same in both spectra, as is the case in Fig. 8, but in principle the spectral width, resolution and the carrier frequency in the F1 domain can also be different for the two experiments. This has an advantage of added flexibility in the experiment setup, but does not necessarily guarantee a perfect and automatic signal alignment.

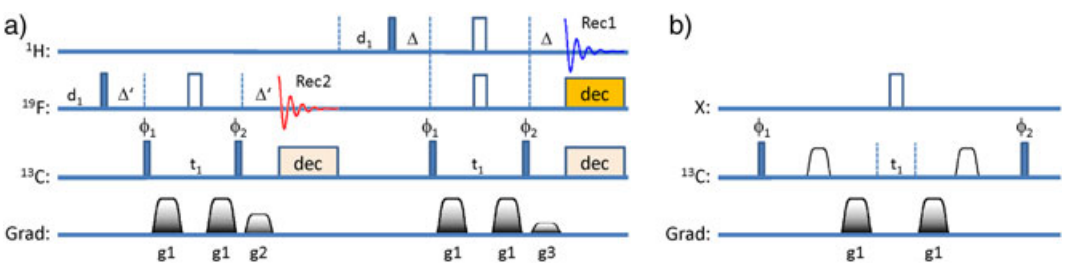

Figure 7. The double-HMQC pulse sequence for recording interleaved H-C and F-C 2D HMQC spectra. The F-C HMQC is shown first to emphasize the longer recovery delay for the H-C HMQC experiment; $\Delta = 0.5/J(HC)$ $\Delta' = 0.5/J(FC)$, all pulses were applied with phase *x*, unless indicated otherwise, $\varphi_1 = x, -x$, $\varphi_2 = x, x, -x, -x$; *Rec1* = *Rec2* = *x*, −*x*, −*x*, *x*; gradients (ms, G/cm): *g1* = (1, 21.4), *g2* = (1, 10.75), *g3* = (1, 11.44); the amplitude of the *g1* gradients was inverted every second scan for echo/anti-echo data in *F1*. The panel (b) shows the implementation of the ^{13}C adiabatic pulses during the t_1 evolution periods; X = ^{1}H and/or ^{19}F, the hollow shaped pulses are 0.5 ms long adiabatic CA WURST-20 pulses[38] covering the active ^{13}C spectral width, gradients and phases are the same as in the main pulse sequence in panel (a).

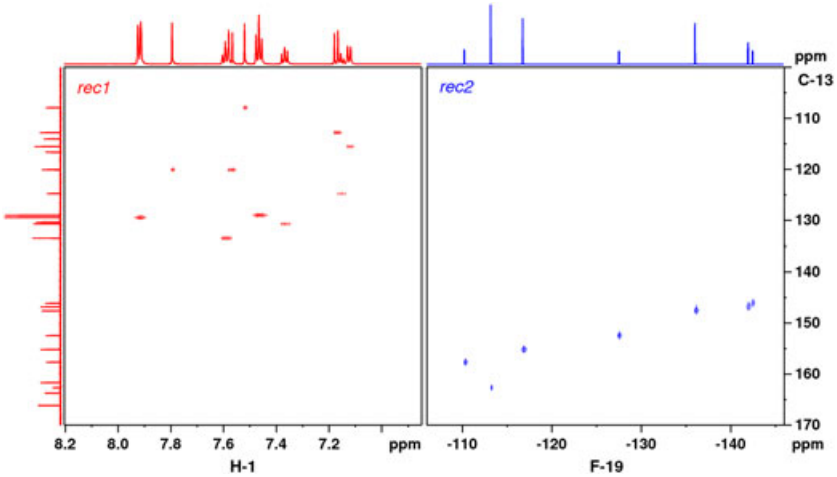

Figure 8. Spectra of a mixture of compounds I-IV (Scheme 1) in DMSO-d_6 (a) H-C HMQC and (b) F-C HMQC – both recorded simultaneously in 7 min using the pulse sequence of Fig. 7 and one scan per increment; experimental parameters: J(HC) = 170 Hz and J(FC) = 250 Hz were used to calculate the Δ and Δ' delays, both d_1 recovery delays were 0.5 s, the acquisition times were 0.366 s (^{1}H) and 0.156 s (^{19}F) resulting in the total recovery period of ca 1.5 s for ^{1}H and 0.5 s for ^{19}F, as discussed in the main text. The spectral width was 4 ppm (^{1}H), 40 ppm (^{19}F) and 80 ppm (^{13}C), and the corresponding raw data matrix size was $2 \times 8\,k \times 256$ data points.

Parallel acquisition experiments

There are two possible arrangements of experiments that are recorded with parallel acquisition of the FIDs – (i) independent experiments with no cross-talk between the two types of nuclei (Fig. 2e) and (ii) experiments that involve coherence transfer between the spin system networks coupled to the directly observed nuclei (Fig. 2f). In the first case the duration of the experiment and hence the time saving as compared with the conventional experiment setup is determined by the recovery time of the slowest relaxing nuclear species. In the second case the experiment duration depends on the properties (T_1 relaxation, abundance, gyromagnetic ratio, γ etc.) of the nuclear species that serve as the polarization source. Both protons and ^{19}F are high-abundance nuclei. The polarization and γ are higher for protons, which are typically favoured as a polarization source. However, the T_1 relaxation is often shorter for ^{19}F nuclei, which reduces the repetition period and therefore increases sensitivity per unit time.

An obvious disadvantage of the parallel acquisition experiments is that the two directly observed nuclear species cannot easily be mutually decoupled when such decoupling is required. It would be rather inconsiderate to say that such mutual decoupling is not possible. Considering that homo-nuclear and hetero-nuclear couplings between protons and ^{19}F are often similar in magnitude adapting some of the homo-decoupling techniques may be of interest in this regard. On the other hand, as shown in the case of multi-receiver experiments involving ^{1}H and ^{13}C nuclei, significant speed advantages over the conventional and interleaved experiments can be achieved in the parallel acquisition experiments that involve polarization transfer from fast relaxing nuclei.

Parallel ^{1}H and ^{19}F T_1 relaxation measurements

Besides a trivial one-dimensional multi-receiver pulse and acquire sequence, the inversion recovery experiment[34] for simultaneous measurement of ^{1}H and ^{19}F T_1 relaxation times represents an example of a parallel acquisition experiment with no coherence transfer between the two nuclei. Therefore, the recycling period in this experiment is defined by the longest of the relaxation times for the two nuclear species. The classical inversion-recovery sequence with parallel acquisition of ^{1}H and ^{19}F FID-s is shown in Fig. 9a. In practice, because of the wide bandwidth of ^{19}F spectrum the rectangular 180° inversion pulses were replaced with short adiabatic pulses (Fig. 9b). Use of wideband inversion pulses is not really necessary for covering the relatively narrow ^{1}H spectral bandwidth. However, the high tolerance of adiabatic pulses towards the RF inhomogeneity and miscalibration makes the experiment more robust and accurate.

The spectra showing the parallel ^{1}H and ^{19}F T_1 measurement for a mixture of fluorinated aromatic compounds I–IV (Scheme 1) are presented in Fig. 10. With the exception of fluoro-benzene, III, the ^{19}F T_1 relaxation times (0.4–0.6 s) in the aromatic compounds I–IV are significantly shorter (by approximately a factor of 6) than those for protons (2.5–4.5 s). Therefore, shorter repetition rates can be

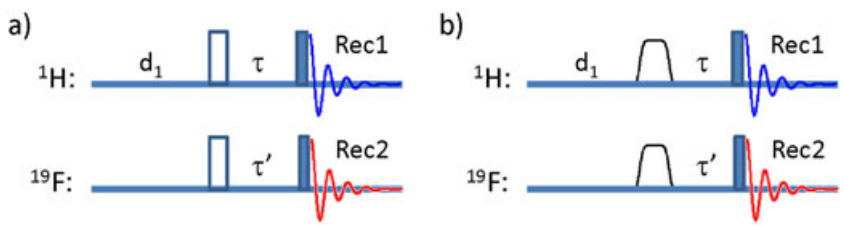

Figure 9. The inversion-recovery pulse sequence for simultaneous measurement of the ^{1}H and ^{19}F T_1 relaxation times on systems equipped with two receivers; (a) with rectangular inversion pulses and (b) with adiabatic pulses; for ^{1}H inversion 500 μs long CA WURST-2 inversion pulses covering a bandwidth of 40 ppm were used whereas for ^{19}F inversion 500 μs long CA WURST-20 pulses covering a bandwidth of 100 ppm were used.

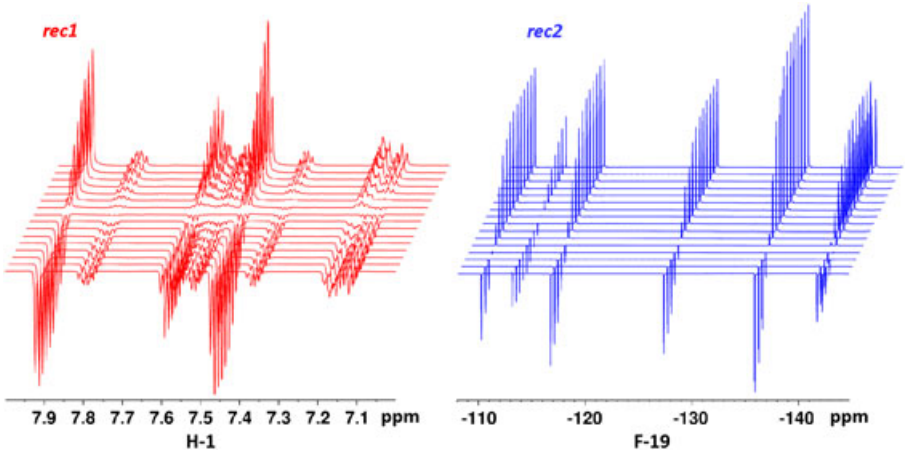

Figure 10. The ^{1}H and ^{19}F inversion-recovery spectra of a mixture containing compounds I–IV (Scheme 1) in DMSO-d_6 recorded simultaneously using the pulse sequence of Fig. 9b. The relaxation period was set to $\tau = \tau' = 0.001$, 0.05, 0.1, 0.2, 0.3, 0.5, 0.8, 1.0, 1.5, 2.0, 2.5, 3.0, 3.5, 4.0, 4.5, 5.0, 6.0, 8.0, 10 and 15 s; the recycling delay, $d_1 = 10$ s, the total measurement time was 29 min.

used and corresponding speed advantages can be achieved in the parallel acquisition experiments with magnetization originating on ^{19}F nuclei.

The short ^{19}F T_1 relaxation times are because of significant contributions from chemical shift anisotropy (CSA) mechanism in addition to the dipole–dipole mechanism that dominates the proton relaxation. The CSA mechanism is associated with the large ^{19}F chemical shift range and scales with the square of the magnetic field strength.[11] In compounds with asymmetric environment around fluorine atoms the CSA contribution induces a significant ^{19}F line broadening at high magnetic fields. In fact, this line broadening may even reduce the resolution achieved by increasing the magnetic field strength. Furthermore, it may also reduce the efficiency of experiments based on polarization transfer via long-range ^{19}F-X couplings (X = ^{1}H, ^{13}C, ^{15}N, ^{19}F, *etc*). On the other hand, in compounds with more symmetric environment, such as fluorobenzene (III) and 2-fluoro-2-deoxy-glucose (V) the contribution from CSA is less significant and the relaxation rates in these compounds for ^{1}H and ^{19}F nuclei are comparable. As demonstrated in the preceding texts the relaxation can have a significant effect on the outcome of experiments discussed here and should be taken into account when optimizing the multi-receiver pulse sequences.

H-H COSY and H-F COSY (PANSY–COSY)

The experiments involving coherence transfer and parallel acquisition of ^{1}H and ^{19}F nuclei typically share the indirectly detected dimension. Generally, the ^{1}H chemical shift range is significantly smaller as compared with that of ^{19}F. Therefore, it may be advantageous to have protons in the F1 domain while maximizing the ^{19}F resolution by direct detection of often huge spectral bandwidth of several tens of kilohertz. The pulse sequence for the H-H/H-F PANSY–COSY experiment[2,39] shown in Fig. 11 is designed to address exactly that type of situation. It is based the conventional COSY pulse sequence with gradient coherence selection.[34] The encoding gradient, *g1*, included in the t_1 evolution period is followed by a read pulse and the decoding gradients, *g2* and *g3* (for simplicity reasons we make no effort to obtain phase sensitive COSY spectra at this point). The decoding gradients are arranged in such a way that the proton magnetization is affected by the sum of *g2* and *g3* gradient area, whereas the ^{19}F nuclei experience only the

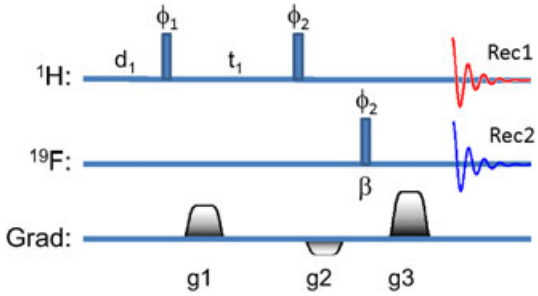

Figure 11. The PANSY–COSY pulse sequence with gradient coherence selection and parallel acquisition of the H-H COSY and H-F COSY; phase cycling: $\varphi_1 = x, -x$; $\varphi_2 = x, x, -x, -x$, *Rec1* = *Rec2* = $x, -x$; gradients (ms, G/cm) *g1* = (1.0, 21.4), *g2* = (1.0, −1.35), *g3* = (1.0, 22.75); flip angle $\beta = 45°$.

g3 gradient. This allows decoding of both the ^{1}H and the ^{19}F detected coherences simultaneously. Note also that the ^{1}H magnetization that is encoded during the t_1 evolution period is split in half by the proton read pulse. Ignoring for a moment the gradient encoding and H-H couplings, it can be shown that the H_zF_z component that would be lost in the conventional COSY experiment here is converted into the H_zF_y magnetization by the ^{19}F read pulse. Unfortunately, the same pulse converts the H_yF_z component into the unobservable H_yF_y magnetization, which can be partially avoided by reducing the flip angle of the ^{19}F pulse to 45° (Fig. 11). Therefore, the sensitivity per unit time in this experiment is the same as if the two 2D spectra were acquired separately, except the spectra are recorded in half the time.

Both the phase-cycled States-TPPI[34] and the echo-anti-echo[34] versions of the pulse sequence were also successfully tested (not shown here). In sensitivity limited situations the phase-cycled version of this experiment (Fig. 1b)[2] may be preferred.

A useful advantage of this type of parallel acquisition experiments is the fact that both spectra share the F_1 frequency axis (Fig. 12), which makes the spectral alignment implicit (automatic) and facilitates the peak assignment in both spectra. Because these experiments effectively correlate three frequencies (H-H-F) they can also be regarded as reduced dimensionality experiments that provide the same information as three-dimensional H-H-F correlation spectra except for the considerably shorter experiment time.[40]

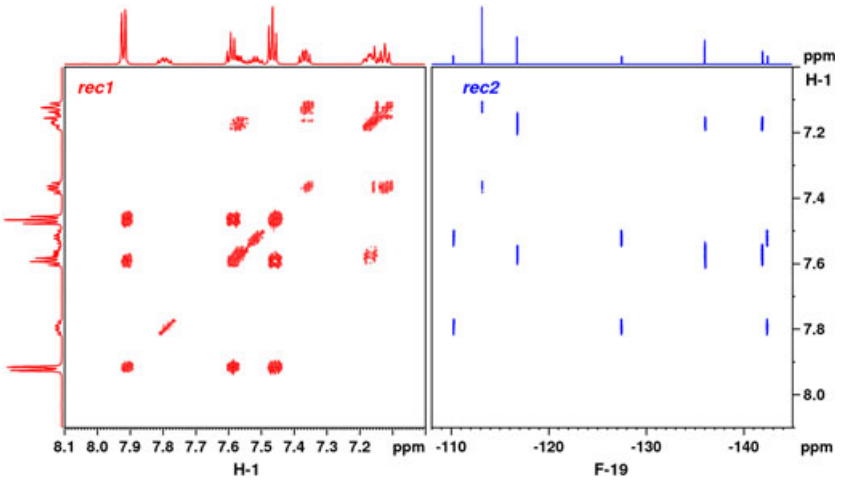

Figure 12. The 2D H-H COSY and H-F COSY spectra of a mixture containing compounds I–IV (Scheme 1) in DMSO-d_6 recorded in parallel using the pulse sequence shown in Fig. 11. The spectral width was 1.6 × 1.6 ppm (H-H COSY) and 50 × 1.6 ppm (F-H COSY) with the corresponding time-domain data matrices ($t_2 \times t_1$) of 1 k (complex) × 256 and 8 k (complex) × 256 data points; $d_1 = 2$ s, 2 scans per increment. The spectra are shown in the absolute value mode, were zero filled to 8 × 1 k and 4 × 1 k sizes correspondingly and processed with sine-bell window functions in both dimensions.

F-F COSY and F-H COSY

The F-F COSY/F-H COSY experiment is very similar to the H-H COSY/H-F COSY experiment, except that ^{19}F is now observed in the joint indirectly detected dimension. In situations where the F-F correlation spectra are of interest, this experiment allows recording of the 2D F-F COSY spectra in parallel with the 2D F-H COSY correlations. In fact, the same pulse programme as for the sequence shown in Fig. 11 can be used except that the gradient ratios are adjusted accordingly (Fig. 13). In this case the ^{19}F nuclei experience the sum of *g2* and *g3* gradient areas, while the ^{1}H nuclei are only affected by the *g3* gradient. Again, the initial ^{19}F magnetization is shared equally by the ^{19}F and ^{1}H detected spectra recovering the information that is lost in the conventional experiments. Both spectra also share the F_1 frequency (^{19}F) axis. As mentioned earlier, the experiment provides the same information as a three-dimensional F-F-H correlation experiment, but in a time of a two-dimensional experiment.

The two spectra recorded for a mixture consisting of compounds I and II (Scheme 1) in DMSO-d_6 using the pulse sequence of Fig. 13 are shown in Fig. 14. Notably, the resolution in the indirectly detected dimension suffers because of the huge ^{19}F spectral bandwidth of 50 ppm (~33 kHz on a 700 MHz instrument). Because the signals are also spread over a wider frequency range this is hardly a problem. Furthermore, a significantly faster repetition rate can be used because of the shorter relaxation time of ^{19}F nuclei in the samples of type that is used here providing further useful time savings in addition to recording two spectra at once. Here we use only 0.2 s recycling delay that delivers the two COSY spectra in just three minutes despite of the huge F1 bandwidth.

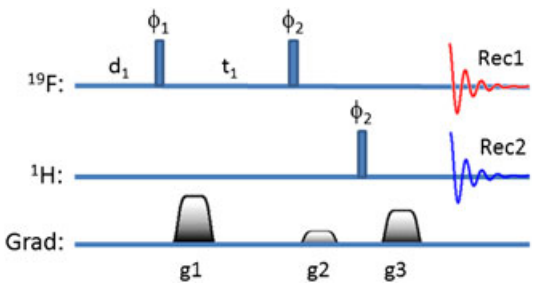

Figure 13. The 2D PANSY–COSY pulse sequence[2,39] with gradient coherence selection for simultaneous recording the F-F COSY and F-H COSY spectral; phase cycling: $\varphi_1 = x, -x$; $\varphi_2 = x, x, -x, -x$, *Rec1* = *Rec2* = $x, -x$; gradients (ms, G/cm) *g1* = (1.0, 21.4), *g2* = (1.0, 1.28), *g3* = (1.0, 20.12).

H,F-X HSQC experiment

Both ^{1}H and ^{19}F nuclei are high-gamma nuclei and can be used as polarization source in correlation experiments with low-gamma insensitive nuclei simultaneously. The pulse sequence for parallel recording of the two-dimensional H-X and F-X correlated HSQC spectra is shown in Fig. 15.[18] In this parallel acquisition experiment the magnetization is transferred from both ^{1}H and ^{19}F nuclei to X nuclei (X = ^{13}C or ^{15}N) and back. Unlike in the COSY-type experiments discussed in the previous section, the magnetization originates and is subsequently directly detected in parallel on both ^{1}H and ^{19}F nuclei essentially independently. Any cross-talk between the ^{19}F and ^{1}H nuclei is minimal because the one-bond ^{1}H-^{13}C and ^{19}F-^{13}C couplings are much larger than the long-range ^{1}H-^{19}F couplings in the test samples studied here (except for the molecule V). Consequently, the repetition rate in this experiment depends on the T_1 of the slowest relaxing nuclei (^{1}H in the test sample used here). The delays and pulses are adjusted to accommodate a substantial difference between the one-bond H-C (~170 Hz) and F-C (~250 Hz) couplings (Fig. 15). There are no coherence gradients in this particular version of the pulse sequence.[18] The sensitivity-enhanced version of this experiment may also be feasible.

The 2D H-C and F-C HSQC spectra of a mixture of 2,3,6-trifluoro-benzoic acid and 2,4,5-trifluoro-benzoid acid (compounds I and II in Scheme 1) in DMSO-d_6 recorded using the PANSY pulse sequence of Fig. 15 are shown in Fig. 16. Note that ^{13}C-decoupling can be used during the acquisition of the ^{1}H and ^{19}F FID-s, but mutual decoupling of ^{1}H and ^{19}F is not feasible in this configuration. In crowded spectra this may be a disadvantage as compared with recording the two spectra as interleaved experiments (refer to the discussion on interleaved 2D H,F-C HMQC experiment). Just like in

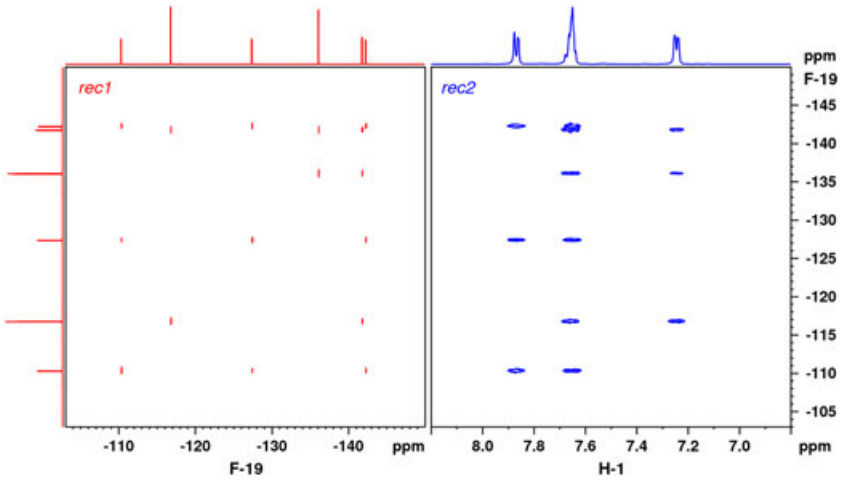

Figure 14. The 2D F-F COSY and H-F COSY spectra of sample 1 recorded simultaneously using the pulse sequence of Fig. 13 on an AV700 MHz system equipped with two receivers and the QCIF CryoProbe; recovery delay, $d_1 = 0.2$ s, 2 scans per increment, 256 increments, the total experiment time was 3 min.

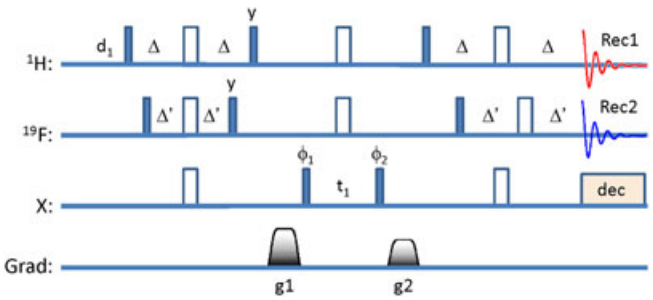

Figure 15. The PANSY H,F-X HSQC experiment for recording two-dimensional H-X and F-X HSQC spectra in parallel (X = ^{13}C or ^{15}N).[18] The filled rectangles represent 90° pulses and hollow rectangles represent 180° pulses. For ^{19}F nuclei pairs of adiabatic pulses were used, as described earlier. All pulses are applied with phase x unless indicated otherwise; phases: $\varphi_1 = x, -x, \varphi_2 = x, x, -x, -x$, *Rec1* = *Rec2* = $x, -x, -x, x$; gradients (ms, G/cm): $g1 = (1, 17)$; $g2 = (1, -15)$.

the interleaved H,F-X HMQC experiment the recovery period in this experiment is defined by the slowest T_1 relaxation of the two nuclei, ^{1}H and ^{19}F.

H,F-X HMBC experiment

The PANSY HMBC experiment is yet another example of how the high polarization from two nuclear species (^{1}H and ^{19}F) can be used for simultaneous recording of two two-dimensional HMBC spectra simultaneously and therefore increase the information content obtained from a single measurement. The PANSY H,F-X HMBC pulse sequence is shown in Fig. 17.[18] It is similar to the HSQC experiment in a sense that the magnetization originates and is subsequently detected on both directly detected nuclei, ^{1}H and ^{19}F, and the two HMBC spectra are recorded in parallel. The delay between the initial 90° excitation pulses on ^{1}H and ^{19}F is adjusted to allow for simultaneous suppression of the one-bond ^{1}H-^{13}C and ^{19}F-^{13}C couplings. This delay is very short (0.95 ms), and hence, the cross-talk between the two nuclear species is negligible. As discussed for the PANSY HSQC experiment in the previous section, the recycling period, d_1, is set according to the relaxation properties of the nuclear species with the longest T_1 relaxation. This PANSY HMBC experiment described here involves coherence selection gradients and therefore must use a γ-filter that separates the ^{1}H and ^{19}F detected experiments in similar with the gradient PANSY

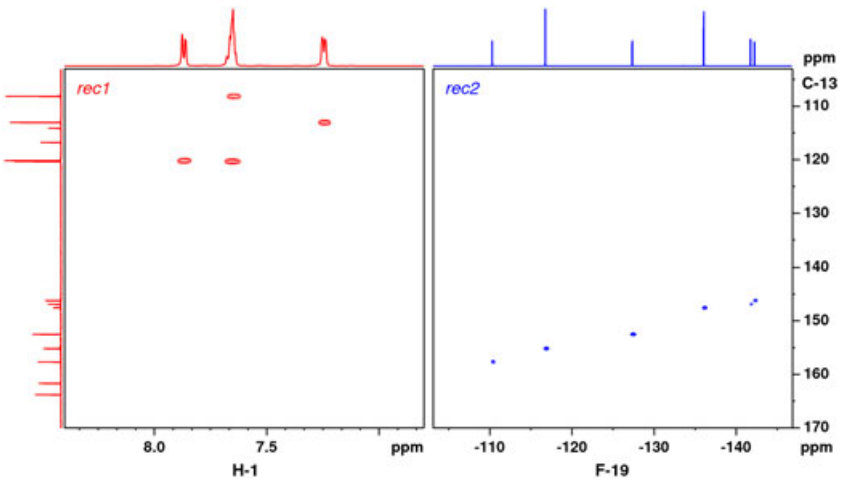

Figure 16. H-C (*Rec1*) and F-C HSQC (*Rec2*) of a mixture of compounds I and II (Scheme 1) in DMSO-d_6 recorded simultaneously using the pulse sequence shown in Fig. 15 on an AV700 MHz spectrometer equipped with two receivers and QCIF CryoProbe; the spectral width was 6 ppm(^{1}H), 44 ppm (^{19}F) and 80 ppm (^{13}C), 256 increments, 2 scans per increment; the total experiment time was 11 min.

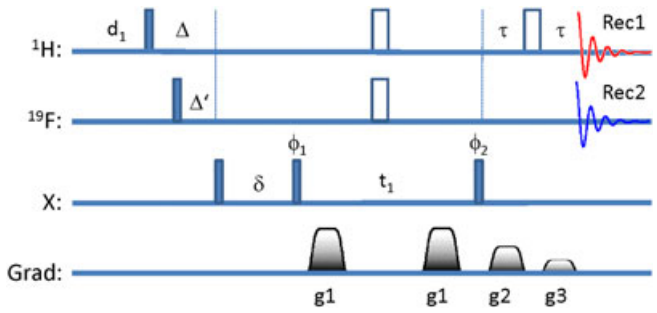

Figure 17. The PANSY H,F-X HMBC experiment for recording two-dimensional H-X and F-X HSQC spectra in parallel (X = ^{13}C or ^{15}N).[18] The filled rectangles represent 90° pulses and hollow rectangles represent 180° pulses. All pulses are applied with phase *x* unless indicated otherwise; phases: $\varphi_1 = x, -x, \varphi_2 = x, x, -x, -x$, *Rec1* = *Rec2* = *x*, −*x*, −*x*, *x*; gradients (ms, G/cm): *g1* = (1, 21.4), *g2* = (1, 11.1), *g3* = (1, 0.34).

COSY experiments discussed in the preceding texts. It consists of a proton refocussing pulse flanked by gradients, *g2* and *g3*. While ^{19}F nuclei experience the sum of the two gradients, the protons experience the difference, *g2* − *g3*. Therefore, gradient selection can be used for simultaneous recording of both the ^{1}H-X and ^{19}F-X HMBC spectra.

The 2D PANSY H,F-C HMBC spectra of a mixture of fluorinated aromatic compounds, I–IV (Scheme 1), recorded using the pulse sequence of Fig. 17 are shown in Fig. 18. The advantages and disadvantages are similar to those discussed for the PANSY HSQC experiment.

Sequential acquisition experiments involving multiple receivers

In some ways the sequential acquisition experiments can be regarded as a compromise between the interleaved and parallel acquisition experiments. Sequential acquisition separates the two direct detection periods allowing at least one of the two directly detected nuclear species to be decoupled from the other. Usually one of the acquisition periods is incorporated into the pulse sequence by making use of long coherence transfer delays. Hence, the sequential acquisition experiments typically involve shared coherence transfer pathways and the associated evolution period(s) in the indirectly detected dimension(s). This is a crucial difference from the interleaved experiments described in the preceding texts.

COCOHOESY–2D H-H COSY and 2D H-F HOESY

The COCOHOESY experiment (Fig. 19) is the hetero-nuclear version of the so called COCONOESY experiment (combined COSY and NOESY)[31] and its solid state analogue.[41] Both, the 2D COSY and the 2D HOESY experiments share the same t_1 evolution period and therefore, the same *F1* frequency axis. Note that the H-H COSY spectrum is acquired during the HOESY mixing period, which typically is much longer that the time required for acquiring the FID in the H-H COSY experiment. Therefore, both the 2D H-H COSY and the 2D H-F HOESY spectra are recorded in the same time duration that normally is required to obtain just the H-F HOESY spectrum

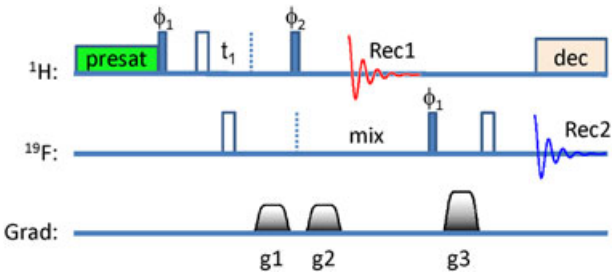

Figure 19. The PANSY H-H COSY and H-F HOESY (COCOHOESY) experiment; all pulses are applied with zero phase unless indicated otherwise; $\varphi_1 = x, -x, \varphi_2 = x, x, -x, -x$, *Rec1* = *Rec2* = *x*, −*x*; gradients (ms, G/cm) *g1* = *g2* = (1.0, 20.13), *g3* = (1.0, 21.40). The polarity of the *g1* gradient was inverted every second increment to produce phase sensitive HOESY spectra; WALTZ-16 proton decoupling was used. In samples with wide ^{19}F bandwidth the rectangular 180° pulses shown as hollow rectangles are replaced with pairs of constant adiabaticity WURST-20 pulses. For recording the F-F COSY and F-H HOESY spectra the *g3* = (1.0, 18.9) and adiabatic decoupling using CA WURST-20 pulses were used (spectra not shown).

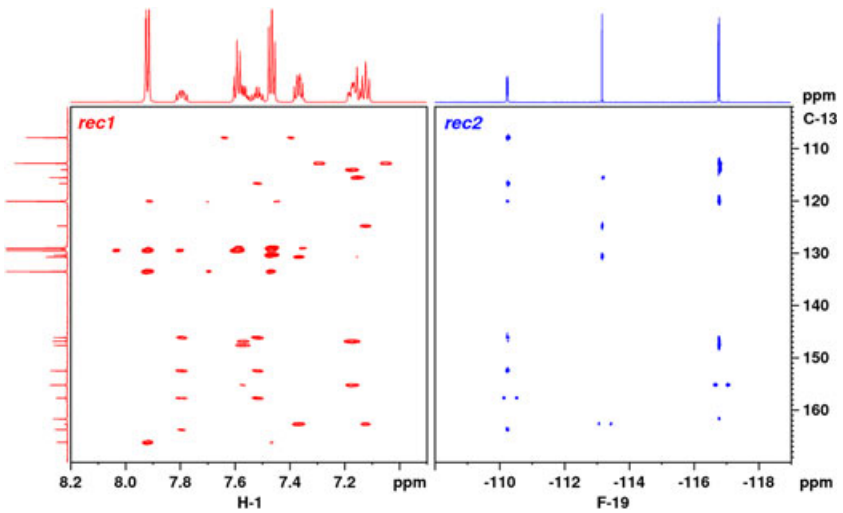

Figure 18. H-C (*Rec1*) and F-C (*Rec2*) 2D PANSY-HMBC spectra of a mixture of compounds I–IV (Scheme 1) in DMSO-d_6 recorded simultaneously on an AV-3HD 700 MHz spectrometer equipped with two receivers and QCIF CryoProbe; 1024 t_1 increments, 2 scans per increment, d_1 = 2 s, total experiment time was 1 h 18 min. For clarity purposes only part of the F-C HMBC spectrum is shown.

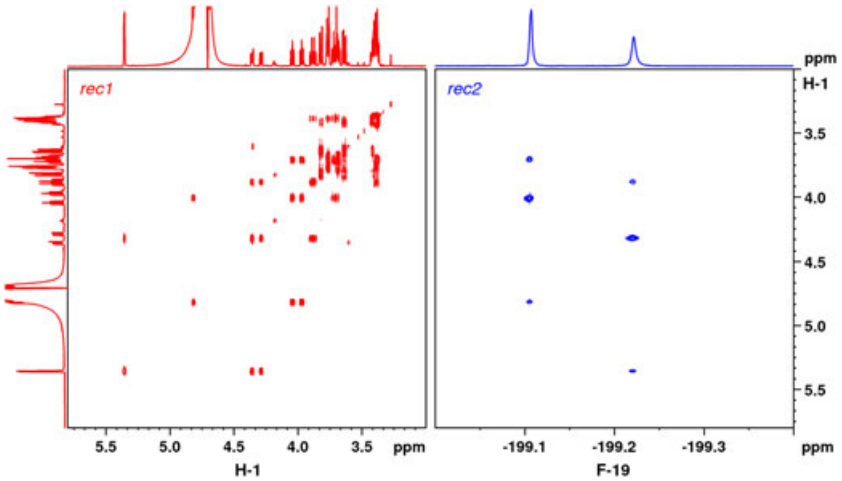

Figure 20. The H-H COSY and F-H HOESY spectra of a mixture of α- and β-2-fluoro-2-deoxy-glucose, recorded using the COCOHOESY pulse sequence of Fig. 19. The acquisition periods were 0.366 s for the ^{1}H detected spectra and 0.623 s for the ^{19}F detected spectra. The acquisition time in the joint ^{1}H t_1-domain was 0.0457 s; the spectral widths ($F_1 \times F_2$) were 4 × 4 ppm (^{1}H) and 4 × 10 ppm (^{19}F); the data matrix sizes ($t_1 \times t_2$) were 2 × 256 k (^{1}H-detected) and 8 × 256 k (^{19}F-detected), one scan per increment, 1.5 s recovery delay, total experiment time for recording the two 2D spectra was 13 min and 8 sec.

by using a single receiver. The gradient selection is achieved by adjusting the *g2* and *g3* gradients according to the gamma ratios of ^{1}H and ^{19}F nuclei correspondingly (see caption to Fig. 19). Here we refocus the ^{19}F magnetization before the start of HOESY acquisition period. Consequently, a phase sensitive 2D H-F HOESY experiment is obtained. The experiment requires a slightly longer recovery delay, if ^{1}H decoupling is used. Considering that the ^{19}F acquisition time in 2D experiments is typically much shorter as compared with the ^{1}H recovery delay, this is a relatively small price to pay for the increased sensitivity and resolution. Besides, it would be the same in the conventional HOESY experiment, and hence, the previously mentioned time savings still apply.

The COCOHOESY spectra of a mixture of α- and β-2-fluoro-2-deoxy-glucose (compound V; Scheme 1) are shown in Fig. 20. In this sample the T_1 relaxation times of ^{1}H and ^{19}F nuclei are comparable. The spectra are essentially identical to those recorded using the conventional pulse sequences (not shown here), but require half the experiment time. In samples with more extensive ^{19}F-^{19}F coupling networks the same pulse sequence can be used to record the F-F COSY and F-H HOESY spectra (not shown here) by simply adjusting the gradient pulses to match the gamma ratios of ^{1}H and ^{19}F nuclei (see caption to Fig. 19). In samples with less symmetric fluorine environment the disadvantage of having a lower starting ^{19}F polarization (as compared with ^{1}H) may be compensated by shorter recycling delays.

PANSY TOCSY experiments

The original 2D PANSY H-H TOCSY/H-X HETCOR experiment was designed with direct detection of ^{1}H and ^{13}C nuclei in mind.[2–5,39] The fluorine-containing compounds typically do not possess any one-bond ^{1}H-^{19}F couplings, and the long-range ^{1}H-^{19}F couplings usually are not suitable for experiments that are based on significant differences between the one-bond and long-range couplings. In such situations the PANSY 2D H-H TOCSY/1D F-19 NMR experiment (Fig. 21a) can be used to acquire a proton decoupled 1D ^{19}F spectrum in parallel with the 2D H-H TOCSY experiment (Fig. 22). In this experiment any cross-talk between ^{1}H and ^{19}F nuclei is suppressed by the ^{19}F refocussing pulse applied in the middle of the t_1 evolution period. Therefore, the 2D HETCOR spectra that are otherwise recorded during the H-H mixing period are replaced with a simple 1D pulse and acquire experiment. This is also an example of simultaneous recording of spectra with different dimensionalities, which is not uncommon in NMR involving multiple receivers.[2–7,18,30,32,33,40] Note that the TOCSY mixing period here acts as a ^{1}H-^{19}F decoupling sequence providing a decoupled 1D ^{19}F spectrum in parallel with the 2D H-H TOCSY spectrum.

The 2D H-H TOCSY/1D ^{19}F {^{1}H} spectra are shown in Fig. 22. Of course, in many cases the 1D ^{19}F spectra can easily be recorded in a single scan. Therefore, the efficiency of this experiment is

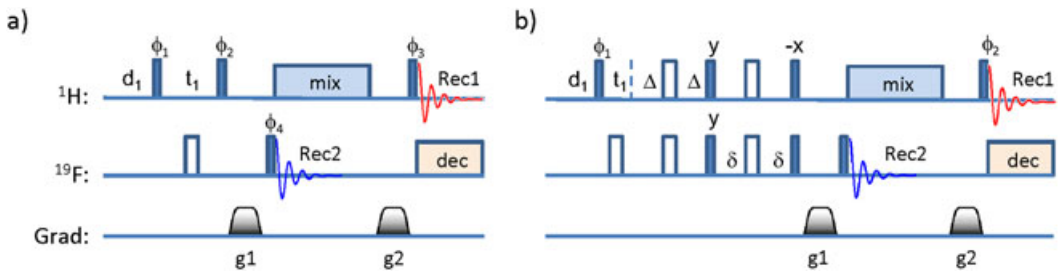

Figure 21. Pulse sequences for recording (a) 2D PANSY H-H TOCSY and 1D ^{19}F spectra, phases, $\varphi_1 = x, -x, \varphi_2 = x, x, -x, -x, \varphi_3 = (x)_4(-x)_4$, *Rec1* = $x, -x, -x, x, -x, x, x, -x, \varphi_4 = Rec2 = x,-x, y, -y$; gradients (ms, G/cm), *g1* = (1.0, 9.5), *g2* = (1.0, 12.7); (b) 2D PANSY H-H TOCSY and 2D H-F HETCOR; $\varphi_1 = x, -x, \varphi_2 = x, x, -x, -x$, *Rec1* = $x,-x, -x, x$, *Rec2* = $x,-x$; the phase φ_1 in both pulse sequences was incremented by 90° every second increment to obtain phase sensitive 2D spectra; all pulses were applied with phase *x* unless indicated otherwise.

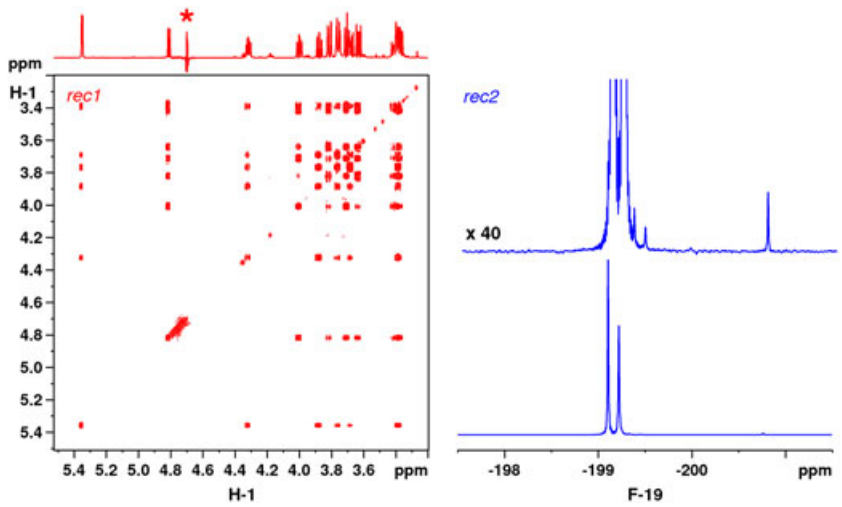

Figure 22. The sequential acquisition (a) 2D H-H TOCSY and (b) 1D ^{19}F NMR spectra of a mixture of α- and β-2-fluoro-2-deoxy-glucose (compound V; Scheme 1) in H_2O/D_2O (9 : 1) recorded using the pulse sequence of Fig. 21a, except that presaturation ($\gamma B_1 = 50$ Hz) was used during the d_1 recovery period; two scans, 256 t_1 increments recorded in 21 min; spectral width was 3.5 kHz (^{1}H, *F1* and *F2*) and 10 kHz (^{19}F). The asterisk in panel (a) indicates the residual water signal. The H-H mixing was implemented using the DIPSI2 sequence,[34] and the ^{1}H decoupled ^{19}F spectrum (b) was recorded during the mixing time of duration, *mix* = 0.11 s; the upper trace in panel (b) shows a vertical expansion by a factor of 40 revealing some minor components in the ^{19}F spectrum;

questionable. However, it may be useful in sensitivity-limited samples, in samples with high dynamic range and if minor components in the F-19 spectra are of interest. For instance, ^{13}C satellites can provide information about the ^{19}F-^{13}C couplings for subsequent HSQC and HMBC experiments and the $^{13/12}$C isotope effects, which amongst other things may explain unusual misalignment of peaks in the 2D correlation spectra and the corresponding (external) 1D projections.

In some cases the geminal ^{19}F-^{1}H couplings can be very different from the other long-range ^{19}F-^{1}H couplings. For instance, in 2-fluoro-2-deoxy-glucose (compound V; Scheme 1) that was used as a test sample here the geminal couplings are in the range of 50 Hz and the PANSY 2D H-H TCOSY and 2D H-F HETCOR experiment (Fig. 21b) can easily be adapted to separate the two-bond H-F correlations from other long-range correlations providing important complimentary information to the H-F COSY experiments described earlier. The PANSY 2D H-H TOCSY and 2D H-F HETCOR spectra are shown in Fig. 23.

There is one important difference from the experiment that was designed for the simultaneous ^{1}H and ^{13}C direct observation.[2] Namely, the ^{13}C is a dilute nuclei and only 1.1% of ^{1}H magnetization is transferred to ^{13}C during the initial INEPT coherence transfer step. In contrast, both ^{1}H and ^{19}F nuclei are abundant, and essentially, all of the (observable) ^{1}H magnetization from the geminal proton(s) is transferred to ^{19}F nuclei in this experiment. As a result, the corresponding traces (rows) in the 2D H-H TOCSY spectrum are 'bleached' out (Fig. 23a). While the F1 traces (columns) still contain all the necessary information, the bleaching effect can easily be avoided by missetting the Δ delay (Fig. 21b). A shorter Δ delay also reduces any weak signals from the leaking through longer-range H-F correlations. On the other hand, a longer Δ delay can be used to enhance the long-range correlations. Noteworthy, the refocussing delay, δ, can also be used for editing purposes to separate the ^{2}J(HF) correlations from the other long-range correlations, mostly via the ^{3}J(FH) couplings. Curiously, longer δ delays make the ^{3}J(FH) correlations appear negative (Fig. 23c). This phenomenon is left unexplained at this point, emphasizing the fact that there is more to be discovered in experiments involving use of multiple receivers.

Combining multi-receiver experiments with other fast techniques

Usually covering vast spectral bands in the indirectly detected dimension requires high number of increments to achieve a reasonable resolution. This, of course, increases the time required to record the spectra. There are several solutions to the problem. Nowadays, one such solution is using non-uniform sampling.[22] This technique can be easily applied to the PANSY HSQC or interleaved HMQC experiments and the data are then processed using the standard software that is available on the commercial state-of-the-art NMR spectrometers. The Projection-Reconstruction method[42] has been used in conjunction with the parallel 3D NMR spectroscopy in bio-molecular solution state NMR.[29,30] Alternatively, one can use the Hadamard encoding[21,39] that is particularly efficient with sparse spectra and huge spectral bandwidth often encountered in ^{19}F NMR.

Hadamard experiments with simultaneous H-1 and F-19 detection

Most of the conventional NMR experiments can be recorded with Hadamard encoding replacing the conventional evolution time and the Hadamard transform replacing the Fourier transform.[21] There are two significant advantages over the conventional NMR spectroscopy – (i) only the real part of the signal in the indirect dimension is required leading to a *sqrt*(2) improvement in sensitivity and a factor of 2 improvement is speed and (ii) the number of increments in the indirectly detected dimension is determined by the number of peaks (adjusted to the nearest multiple of 4), which in sparse spectra leads to further significant time savings. A prior knowledge of peak positions is required, which in the case of ^{1}H and ^{19}F experiments is easily obtained from the initial 1D measurements.

The pulse sequence for recording the 2D Hadamard PANSY-COSY spectra (Fig. 24) is a simple modification of the gradient PANSY-COSY pulse sequence shown in Fig. 13. The Hadamard encoding pulse is usually a simple 90° Gaussian pulse and is chosen because of the high phase gradient across the excitation bandwidth.[21] This allows the scalar H-F and H-H couplings to

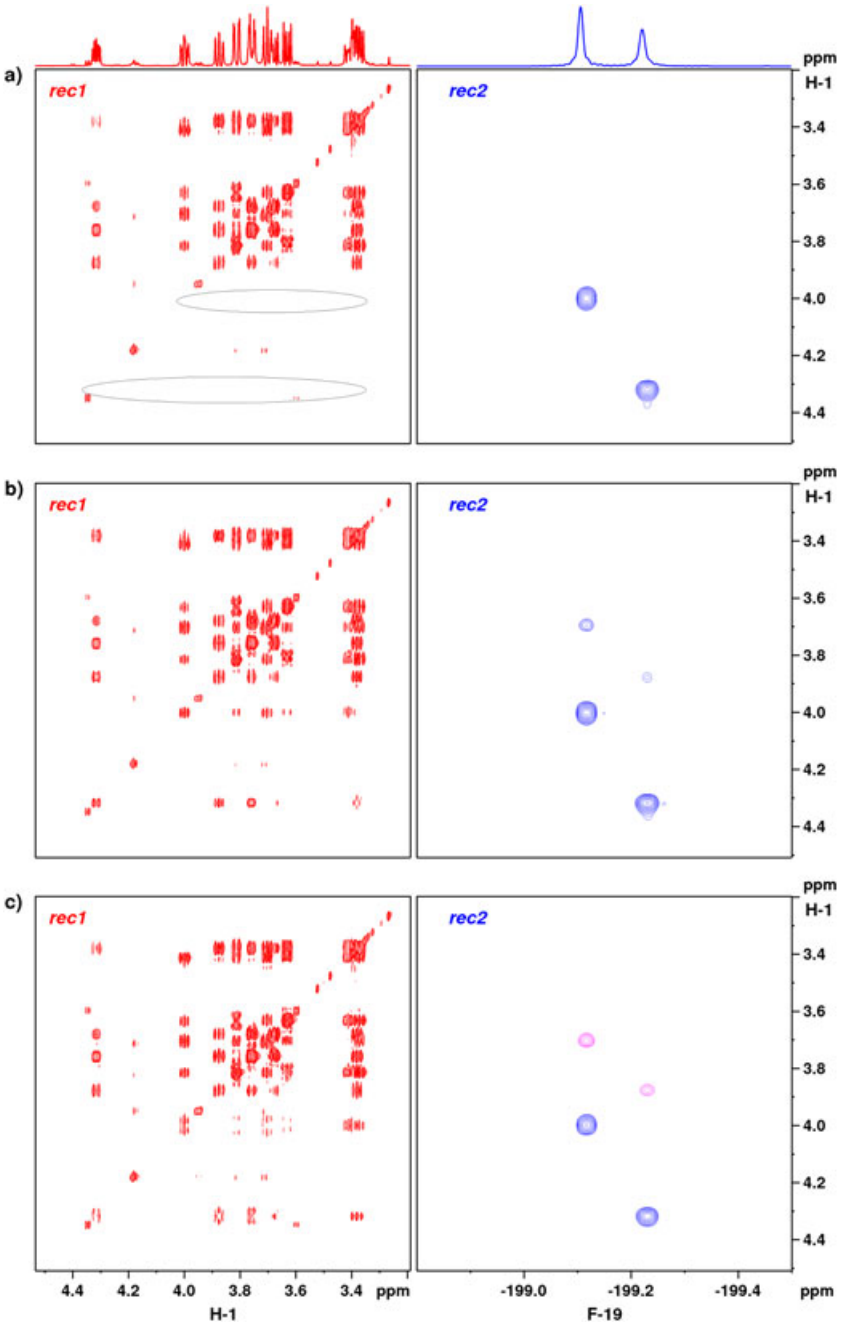

Figure 23. The sequential acquisition 2D PANSY H-H TOCSY (left) and H-F HETCOR (right) spectra of a mixture of α- and β-2-fluoro-2-deoxy-glucose (compound V; Scheme 1) in H_2O/D_2O (9 : 1) recorded simultaneously using the pulse sequence of Fig. 21b, except that presaturation ($\gamma B_1 = 50$ Hz) was used during the d_1 recovery period; two scans, 256 t_1 increments recorded in 21 min; spectral width was 3.5 kHz (^{1}H, *F1* and *F2*) and 10 kHz (^{19}F, *F1*). The *J* (HF) evolution delays were set to (a) $\Delta = 5$ ms, $\delta = 5$ ms; (b) $\Delta = 2.5$ ms, $\delta = 2.5$ ms; and (c) $\Delta = 2.5$ ms, $\delta = 7$ ms. The bleached out regions in the top left panel are indicated by circles. The weaker three-bond correlations and the bleached TOCSY peaks in the bottom panels appear negative and in the electronic version of this figure are displayed in purple.

evolve during the pulse so that no additional J evolution period is required. The duration of this pulse is adjusted accordingly to emphasize transfer via larger or smaller J couplings as required. Unfortunately, this also slightly changes the excitation bandwidth and a compromise setting may be required. However, for the well-dispersed ^{19}F spectra this is usually not a problem. The Hadamard version of the F-F and F-H PANSY COSY spectra for a mixture of compounds I and II (Scheme 1) are shown in Fig. 25.

The sensitivity of the F-H correlated experiments is usually sufficiently high to allow recording the gradient version of the Hadamard PANSY COSY spectra with a single scan per increment. Consequently, such correlation spectra can be obtained very quickly. Furthermore, as described in the preceding texts in the case of the conventional F-H PANSY COSY experiment the short ^{19}F T_1 relaxation times in the sample used here (a mixture of compounds I and II; Scheme 1) can be exploited to reduce the recycling delay d_1, which permits recording of the two 2D PANSY COSY experiments in just 3 s or less (Fig. 25).

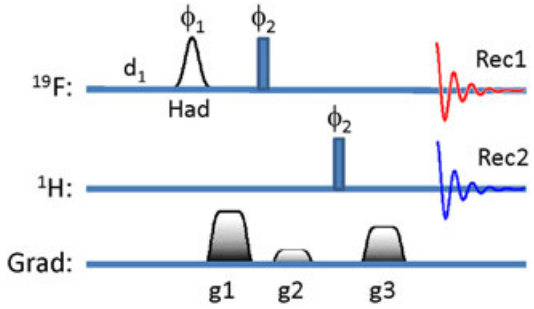

Figure 24. The 2D Hadamard F-F COSY and F-H COSY (Hadamard PANSY-COSY) experiment with gradient coherence selection. The Hadamard encoding pulse of Gaussian shape was 37.4 ms long and replaces the first hard pulse and the t_1 evolution delay in the conventional pulse sequence shown in Fig. 13. Other experimental details are the same.

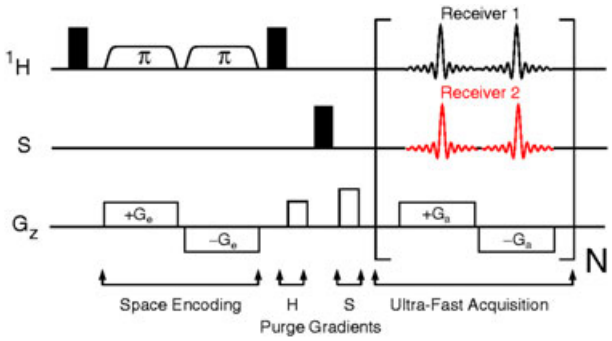

Figure 26. The pulse sequence for parallel acquisition of ultra-fast 2D F-F COSY and H-F COSY spectra (PUFSY) Reproduced from *Angew. Chem. Int. Ed.* **2013**, *52*, 4152–4155 with permission.

Ultra-fast H-H COSY and H-F COSY (PUFSY)

The ultra-fast (UF) NMR spectroscopy introduced by Frydman *et al*[26,27] is based on spatial frequency encoding in the F1 domain, which replaces the traditional t_1 evolution period achieving two-dimensional NMR correlation spectroscopy in a single scan. The UF version of the PANSY H-H COSY and H-F COSY experiment[19] is shown in Fig. 26. In this particular example the joint F1 (proton) frequency domain is encoded using the constant time method[43] that involves two adiabatic 180° (WURST) pulses in the presence of a bipolar gradient pulse, $\pm G_e$. The coherence selection is achieved by two purge gradients, H and S in a similar fashion to that described for the conventional PANSY COSY experiment described in the preceding texts. This allows simultaneous detection of both the ^{1}H and ^{19}F FIDs in the presence of a decoding bipolar gradient waveform, $\pm G_a$. Consequently, an UF 2D H-H COSY spectrum from receiver 1 can be recorded in parallel with a hetero-nuclear UF 2D H-F COSY spectrum in receiver 2 in about 105 ms. The experiment has been named PUFSY – Parallel Ultra-Fast SpectroscopY.

The H-F PUFSY spectra of a mixture consisting of 2,3,6-trifluoro benzoic acid, 2,4,5-trifluoro benzoic acid and 2,3,4-trifluoro cinnamic acid in DMSO-d_6 recorded using the pulse sequence of Fig. 26 are shown in Fig. 27. Note that because the same decoding gradients $\pm G_a$ are simultaneously experienced by both nuclear species during the direct detection period, the same absolute spectral width (in Hz) in the direct detection domain applies to the F2 frequency axis in both H-H and H-F correlated spectra. In addition, computer optimized folding[23,24] was used in the ^{19}F domain to accommodate the large frequency range of ~25 kHz on a 600 MHz NMR system. All the expected peaks were observed in these spectra. The main limitation of this technique is the relatively low sensitivity as is generally the case with the UF experiments. On the other hand, as discussed earlier, more signal and more information is obtained in this parallel UF experiment as compared with the corresponding individual single receiver experiments. The same pulse sequence has been used to record also the H-P correlated PUFSY experiments.[19]

Conclusions

We show that many of the basic 2D experiments, such as COSY, TOCSY, HOESY, HETCOR, HSQC, HMBC, HMQC, DOSY and T_1 measurements by the inversion recovery method, that are routinely used in NMR of small molecules can easily be adapted for simultaneous direct observation of two or more abundant and sensitive

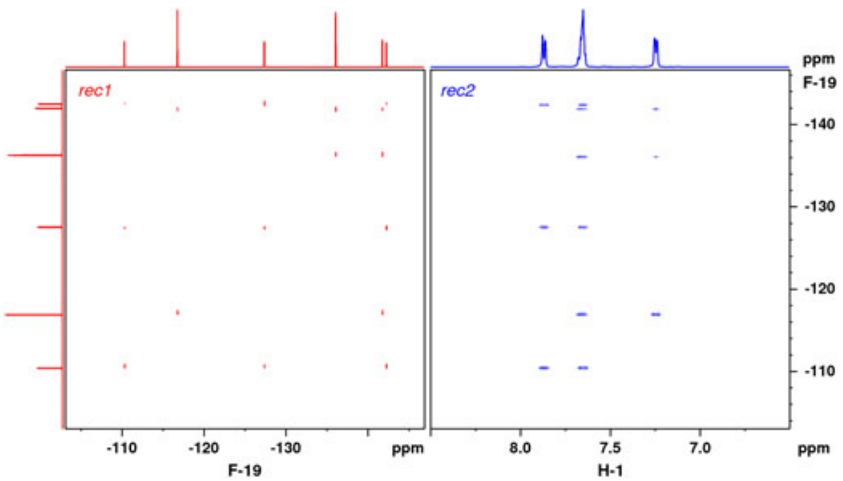

Figure 25. The 2D Hadamard F-F COSY and F-H COSY spectra of a mixture containing compounds I and II (Scheme 1) recorded in parallel on an AV700 MHz spectrometer equipped with two receivers and QCIF CryoProbe. Both spectra were recorded simultaneously using a recycling delay of $d_1 = 0.2$ s, H8 encoding matrix, one scan per increment and a total of eight increments. The total experiment time was 3 s.

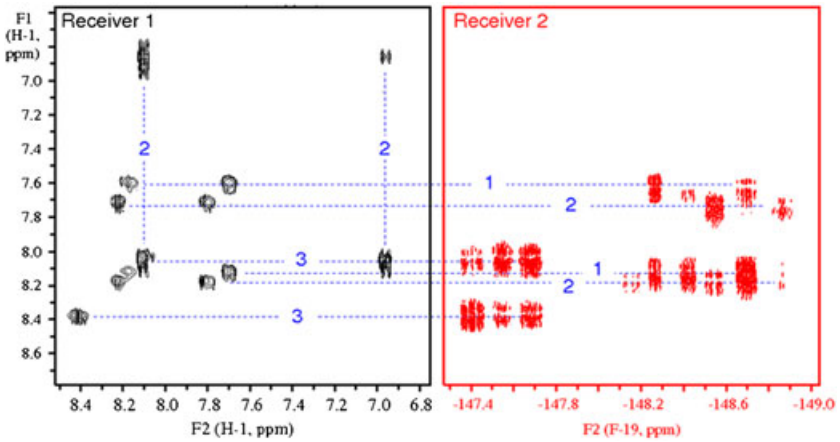

Figure 27. The ultra-fast 2D F-F COSY and H-F COSY spectra (PUFSY) of a mixture consisting of 2,3,6-trifluoro-benzoic acid, 2,4,5-trifluoro-benzoic acid and 2,3,4-trifluoro-cinnamic acid in DMSO-d_6 recorded in parallel using the pulse sequence shown in Fig. 26 in 105 ms. Reproduced from *Angew. Chem. Int. Ed.* **2013**, *52*, 4152–4155 with permission.

nuclei, such as ^{1}H, ^{19}F and ^{31}P resulting in significant time savings, which potentially can double the throughput and efficiency in many analytical NMR laboratories. We present many such examples involving ^{1}H and ^{19}F nuclei and have also successfully tested similar experiments involving ^{1}H and ^{31}P nuclei (not shown here).

We categorize the multi-receive experiments discussed in this work into three main types – interleaved experiments, parallel acquisition experiments and sequential acquisition experiments. Each of these types may have different sub-types of experiments depending on the relaxation properties of the involved nuclei, decoupling requirements, the involved spin systems and the associated coherence transfer pathways.

In addition to the significant time savings the higher efficiency of multi-receive experiments is also helped by the fact that only one experiment needs to be set up in order to record several multi-dimensional spectra. Furthermore, the multi-receive experiments can be arranged to avoid potential redundancy in spectral information content. For instance, 2D PANSY H-H,F COSY, F-F,H COCOHOESY, HF-X (X = ^{13}C or ^{15}N) HSQC and HMBC, H-H,F PANSY-TOCSY, H,F-DOSY and H,F inversion recovery experiments all provide complementary information. Many of these experiments are amenable to further reduction of experiment time by using fast NMR techniques, such as Hadamard NMR, non-uniform sampling, spatial encoding or fast pulsing approaches.

In this work we have explored only the very basic small molecule experiments sometimes keeping the level of sophistication low for illustrative purposes. Not only there are many extensions and improvements that can be implemented based on the provided examples, but many other more sophisticated experiments can be converted into more efficient pulse sequences that take advantage of the multiple receiver technology. Furthermore, the provided examples clearly demonstrate that the multi-receive experiments can be further optimized taking into consideration the relaxation properties of the involved nuclei. The possible configurations of such experiments have been discussed, and the advantages and disadvantages of the individual types and implementations have been highlighted.

Apart of straightforward efficiency and throughput improvements, there are other potentially very interesting areas of application of multi-receiver technology. For instance, development of new experiments and pulse sequences, following the coherence flow in complex multi-dimensional experiments involving multi-nuclear spin systems and networks can all be made significantly more efficient and simpler by having the ability to observe the magnetization on any channel at any point in the experiment facilitating discoveries of new NMR phenomena. While we have only touched the tip of the 'iceberg' in small molecule NMR, the same principles apply to many bio-molecular experiments involving labelled protein and RNA samples.[4–7,29,30,40] Balancing the sensitivity of high and low gamma nuclei in such experiments pose further challenges in multi-receive pulse sequence design.

Finally, we believe that the multi-receiver technology will boost the development of new NMR experiments and NMR research in general, making the NMR instruments more efficient and making the NMR spectroscopy even more unique in the universe of analytical tools and experimental techniques.

References

[1] R. Petkewich. *C&E News* **2008**, *86*, 10.
[2] Ē. Kupče, R. Freeman, B. K. John. *J. Am. Chem. Soc.* **2006**, *128*, 9606–9607.
[3] Ē. Kupče, R. Freeman, in *Modern NMR Approaches for the Structure Elucidation of Natural Products*, vol. *1* (Eds: A. Williams, G. Martin), RSC Publishing, London, **2015**, pp. 119–145.
[4] Ē. Kupče. *eMagRes* **2015**, *4*, 721–732. doi:http://dx.doi.org/10.1002/9780470034590.emrstm1404.
[5] Ē. Kupče. *Top. Curr. Chem.* **2013**, *335*, 71–96.
[6] J. G. Reddy, R. V. Hosur. *J. Struct. Funct. Genomics* **2014**, *14*, 25–32.
[7] S. M. Pudakalakatti, A. Dubey, G. Jaipuria, U. Shubhashree, S. K. Adiga, D. Moskau, H. S. Atreya. *J. Biomol. NMR* **2014**, *58*, 165–173.
[8] C. Martineau, F. Decker, F. Engelke, F. Taulelle. *Solid State NMR* **2013**, *48*, 55–56.
[9] M. Pellecchia, I. Bertini, D. Cowburn, C. Dalvit, E. Giralt, W. Jahnke, T. L. James, S. W. Homans, H. Kessler, C. Luchinat, B. Meyer, H. Oschkinat, J. Peng, H. Schwalbe, G. Siegal. *Nat. Rev. Drug Discov.* **2008**, *7*, 738–745.
[10] D. A. Erlanson, W. Jahnke, R. Mannhold, H. Kubinyi, G. Folkers, *Fragment-based Drug Discovery: Lessons and Outlook*, John Wiley & Sons Ltd, Chichester, **2016**.
[11] J. L. Kitevski-LeBlanc, R. S. Prosser. *Prog. NMR Spectrosc.* **2012**, *62*, 1–33.
[12] J.-X. Yu, R. R. Hallac, S. Chiguru, R. P. Mason. *Prog. NMR Spectrosc.* **2013**, *70*, 25–49.
[13] J. Wang, M. Sánchez-Roselló, J. L. Aceña, C. del Pozo, A. E. Sorochinsky, S. Fustero, V. A. Soloshonok, H. Liu. *Chem. Rev.* **2014**, *114*, 2432–2506.
[14] J. Swinson. *Pharma. Chem.* **2005**, June, 26–27.
[15] D. O'Hagan. *J. Fluor. Chem.* **2010**, *131*, 1071–1108.
[16] C. Dalvit. *Concepts in Magn. Reson., Part A* **2008**, *32*, 341–372.
[17] J. Battiste, R. A. Newmark. *Prog. NMR Spectrosc.* **2006**, *48*, 1–23.

[18] Ē. Kupče, S. Cheatham, R. Freeman. *Magn. Reson. Chem.* **2007**, *45*, 378–380.
[19] K. J. Donovan, Ē. Kupče, L. Frydman. *Angew. Chem. Int. Ed.* **2013**, *52*, 4152–4155.
[20] Ē. Kupče, R. Freeman. *J. Magn. Reson.* **2011**, *213*, 1–13.
[21] Ē. Kupče, T. Nishida, R. Freeman. *Prog. NMR Spectrosc.* **2003**, *42*, 95–122.
[22] S. G. Hyberts, H. Arthanari, G. Wagner. *Top. Curr. Chem.* **2012**, *316*, 125–148.
[23] D. Jeannerat. *Magn. Reson. Chem.* **2003**, *41*, 3–17.
[24] E. Lescop, P. Schanda, R. Rasia, B. Brutscher. *J. Am. Chem. Soc.* **2007**, *129*, 2756–2757.
[25] P. Schanda, B. Brutscher. *J. Am. Chem. Soc.* **2005**, *127*, 8014–8015.
[26] L. Frydman, T. Scherf, A. Lupulescu. *Proc. Natl. Acad. Sci. U. S. A.* **2002**, *99*, 15,858–15,862.
[27] A. Tal, L. Frydman. *Prog. NMR Spectrosc.* **2010**, *57*, 241–292.
[28] A. Viegas, T. Viennet, T.-Y. Yu, F. Schumann, W. Bermel, G. Wagner, M. Etzkorn. *J. Biomol. NMR* **2016**, *64*, 1–7.
[29] Ē. Kupče, L. E. Kay. *J. Biomol. NMR* **2012**, *54*, 1–7.
[30] Ē. Kupče, L. E. Kay, R. Freeman. *J. Am. Chem. Soc.* **2010**, *132*, 18,008–18,011.
[31] A. Z. Gurevich, I. L. Barsukov, A. S. Arseniev, V. F. Bystrov. *J. Magn. Reson.* **1984**, *56*, 471–478.
[32] Ē. Kupče, R. Freeman. *J. Am. Chem. Soc.* **2008**, *130*, 10,788–10,792.
[33] Ē. Kupče, R. Freeman. *J. Magn. Reson.* **2010**, *206*, 147–153.
[34] J. Keeler, *Understanding NMR Spectroscopy*, John Wiley and Sons Ltd, Chichester, **2005**.
[35] K. F. Morris, C. S. Johnson Jr.. *J. Am. Chem. Soc.* **1992**, *114*, 3139–3141.
[36] C. S. Johnson Jr.. *Prog. NMR Spectrosc.* **1999**, *34*, 203–256.
[37] [37] C. Xu, Y. Wan, D. Chen, C. Gao, H. Yin, D. Fetherston, Ē. Kupče, G. Lopez, B. Ameduri, E. Twum, F. J. Wyzgoski, X. Li, E. F. McCord, P. L. Rinaldi. *Magn. Reson. Chem.* **2016** in press.
[38] Ē. Kupče, R. Freeman. *NMR Biomed.* **1997**, *10*, 372–380.
[39] P. Gierth, A. Codina, F. Schumann, H. Kovacs, Ē. Kupče. *Magn. Reson. Chem.* **2015**, *53*, 940–944.
[40] J. G. Reddy, R. V. Hosur. *J. Biomol. NMR* **2013**, *56*, 77.
[41] K. Takeda, Y. Kusakabe, Y. Noda, M. Fukuchi, K. Takegoshi. *Phys. Chem. Chem. Phys.* **2012**, *14*, 9715–9721.
[42] Ē. Kupče, R. Freeman. *J. Am. Chem. Soc.* **2004**, *126*, 6429–6440.
[43] P. Pelupessy. *J. Am. Chem. Soc.* **2003**, *125*, 12,345–12,350.